Photoelectrolysis

Deutsche Ausgabe: DOI: 10.1002/ange.201703326
Internationale Ausgabe: DOI: 10.1002/anie.201703326

Iron Oxide Photoelectrode with Multidimensional Architecture for Highly Efficient Photoelectrochemical Water Splitting

Jin Soo Kang, Yoonsook Noh, Jin Kim, Hyelim Choi, Tae Hwa Jeon, Docheon Ahn, Jae-Yup Kim, Seung-Ho Yu, Hyeji Park, Jun-Ho Yum, Wonyong Choi, David C. Dunand, Heeman Choe, and Yung-Eun Sung**

Abstract: *Nanostructured metal oxide semiconductors have shown outstanding performances in photoelectrochemical (PEC) water splitting, but limitations in light harvesting and charge collection have necessitated further advances in photoelectrode design. Herein, we propose anodized Fe foams (AFFs) with multidimensional nano/micro-architectures as a highly efficient photoelectrode for PEC water splitting. Fe foams fabricated by freeze-casting and sintering were electrochemically anodized and directly used as photoanodes. We verified the superiority of our design concept by achieving an unprecedented photocurrent density in PEC water splitting over 5 mA cm^{-2} before the dark current onset, which originated from the large surface area and low electrical resistance of the AFFs. A photocurrent of over 6.8 mA cm^{-2} and an accordingly high incident photon-to-current efficiency of over 50% at 400 nm were achieved with incorporation of Co oxygen evolution catalysts. In addition, research opportunities for further advances by structual and compositional modifications are discussed, which can resolve the low fill factoring behavior and improve the overall performance.*

Owing to the rapidly increasing demands on sustainable hydrogen production, intensive efforts have been devoted for the utilizations of solar energy for water electrolysis.[1–3] For effcient solar water splitting, developement of photocatalysts or combinations of photovoltaic and water electrolyzer has been performed and significant advances have been achieved.[4–9] Additionally, water photoelectrolysis based on photoelectrochemical (PEC) water splitting is receiving much attention owing to its superior characteristics such as feasible solar-to-hydrogen conversion in a single device that enables direct collection of H_2 without separation from evolved oxygen in industrially optimized systems.[10–12]

For the PEC water splitting, there have been numerous reports on the design and preparation of nanostructured metal oxide semiconductor photoelectrodes. Since the pioneering work employing titania,[13] various metal oxides, such as TiO_2,[14–16] WO_3,[17,18] Cu_2O,[19,20] $BiVO_4$,[21–23] and α-Fe_2O_3[24–33] have been frequently used as photoelectrodes. Among these, α-Fe_2O_3 is considered to be one of the most attractive oxides for water photoelectrolysis, because it is chemically stable, environmentally favorable, and earth-abundant. A number of nanostructures with appropriate dopants were proposed to enhance the performance but there are still plenty of opportunities for further advances.[29,34]

Herein, we propose anodized Fe foam (AFF) as a new type of photoelectrodes and investigate its application for PEC water splitting. We designed the photoanodes to have the following ideal characteristics: 1) large surface area for light harvesting, 2) low-dimensionally confined semiconductor structure for enhanced charge transport, and 3) three-dimensionally extended current collector with very low resistance. By anodic oxidation of Fe foams, which were prepared by freeze-casting,[35,36] vertically aligned iron oxide nanoflakes were synthesized on the Fe foam surfaces. AFFs in PEC water splitting generated large photocurrents, verifying the general advantages of this design concept.

AFF photoelectrodes were prepared by electrochemical anodic oxidation of freeze-cast Fe foam (Figure 1 a), for which a modified procedure of the method in previous reports was

[*] Dr. J. S. Kang, J. Kim, Dr. S.-H. Yu, Prof. Y.-E. Sung
Center for Nanoparticle Research, Institute for Basic Science (IBS)
Seoul 08826 (Republic of Korea)
and
School of Chemical and Biological Engineering, Seoul National University, Seoul 08826 (Republic of Korea)
E-mail: ysung@snu.ac.kr

Y. Noh, Dr. H. Choi, H. Park, Prof. H. Choe
School of Advanced Materials Engineering, Kookmin University
Seoul 02707 (Republic of Korea)
E-mail: heeman@kookmin.ac.kr

T. H. Jeon, Prof. W. Choi
Division of Environmental Science and Engineering
Pohang University of Science and Technology (POSTECH)
Pohang 37673 (Republic of Korea)

Dr. D. Ahn
Beamline Department, Pohang Accelerator Laboratory (PAL)
Pohang 37673 (Republic of Korea)

Prof. J.-Y. Kim
Department of Chemical Engineering, Hoseo University
Asan 31499 (Republic of Korea)

Dr. J.-H. Yum
Laboratory for Molecular Engineering of Optoelectronic Nanomaterials, École Polytechnique Fédérale de Lausanne (EPFL)
Station 6, 1015 Lausanne (Switzerland)

Prof. D. C. Dunand
Department of Materials Science and Engineering, Northwestern University, Evanston, IL 60208 (USA)

Prof. H. Choe
Cellmotive Co. Ltd., Kookmin University
Seoul 02707 (Republic of Korea)

Supporting information and the ORCID identification number(s) for the author(s) of this article can be found under: https://doi.org/10.1002/anie.201703326.

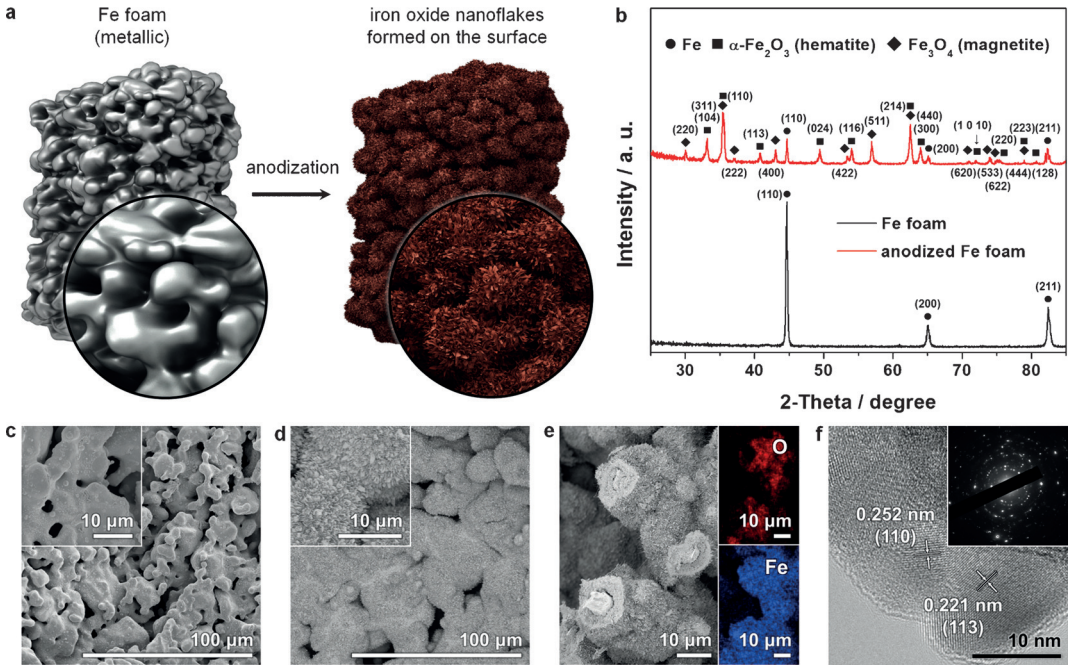

Figure 1. a) Schematic image displaying the preparation of an AFF photoanode and b) XRD data of Fe foam before and after anodization followed by heat treatment at 500 °C for 4 h. XRD peaks were assigned according to JCPDS 06-0696 (Fe), 33-0664 (α-Fe_2O_3), and 19-0629 (Fe_3O_4). SEM images of c) Fe foam and d,e) anodized Fe foam. f) TEM image and SAED patterns (inset) of iron oxide on the surface of AFF.

used;[37,38] applying 80 V for 5 min at 25 °C using an ethylene glycol electrolyte containing 0.25 wt % NH_4F and 2 vol% H_2O with the assistance of ultrasonication. The X-ray diffraction (XRD) patterns displayed in Figure 1 b show the formation of iron oxide by the anodization process, and the scanning electron microscope (SEM) analyses (Figure 1 c,d and Figure S1 in the Supporting Information) revealed that two-dimensional iron oxide nanoflakes were formed on the surface of the Fe foam. The SEM image of a fracture surface shown in Figure 1 e suggests that the oxide layer, including the nanoporous oxides below the flakes (see Figure S3), is ca. 2 μm in thickness. Additionally, the existence of Fe metal beneath the iron oxide is observable in the SEM image and corresponding energy dispersive spectroscopy (EDS) mapping results displayed on the insets of Figure 1 e. This implies that Fe metal underneath the Fe oxide may serve as the current collector. The internal part (near the center) of the AFF did not exhibit a specific difference in morphology compared to the external region (Figure S2). In addition, together with the XRD pattern (Figure 1 b), transmission electron microscope (TEM) image (Figure 1 f) and selected area electron diffraction (SAED) pattern (inset of Figure 1 f) confirm that the iron oxide is mainly hematite with the presence of a secondary magnetite phase. The average crystallite size was 24 nm, as calculated from the Scherrer's equation and the (110) peak of α-Fe_2O_3.

Meanwhile, it is clearly observable that nanoflake morphology is diverse considering the nanoporous or nanotubular structures in previous reports on anodic iron oxides.[28,39,40] Therefore, investigations on the relationship between anodizing conditions and oxide nanostructure were performed based on previous studies.[41–45] In general, formation of anodic oxide films on metal substrate is based on the equilibrium between metal oxide formation by electric potential and chemical dissolution of oxides by the electrolyte, which usually contains F^- and H_2O.[41,42] The etching process of metal oxides comprises a number of steps; formation of M-OH^{2+} by protonation of metal oxide ligand, replacement of $-OH^{2+}$ by $-F_x$, and nucleophilic substitution that removes the $M-F_x$ unit from the metal oxide lattice.[45] In the $M-F_x$ formation step, the presence of HF and its derivatives (HF_2^- and H_2F_2) is essential, and in the case of anodization using H_2O and F^--containing electrolyte, H^+ from water dissociation caused by the large applied potential induces formation of HF, HF_2^-, and H_2F_2.[43,45] For this reason, the electrolyte composition is a critical factor that affects the final morphologies of anodic oxide films. Based on this understanding of anodic oxidation, we performed anodization of Fe foil using electrolytes with four different compositions described in Table S1. Interestingly, as the overall concentration of the electrolyte and NH_4F to H_2O ratio increased, anodic iron oxide with various nanostructures ranging from nanoflakes to nanotubes were synthesized as shown in Figure 2. These results indicate that the structures of anodic iron oxides can be modified by varying the electrochemical environments that are easily controlled by electrolyte compositions. We could thereby attribute the nanoflake structures to the anodization condition that Fe foam experience during anodic oxidation that are possibly milder than the case of Fe foil due to the porous stucture and large surface area.

The performance of the AFF as a photoanode for water photoelectrolysis characterized under AM 1.5G illumination using 1 M NaOH solution as the electrolyte is displayed in Figure 3 a. We confirmed that the spectral intensity of the solar simulator matches well with the standard AM 1.5G spectrum (Figure S4) and obtained the photocurrent density–

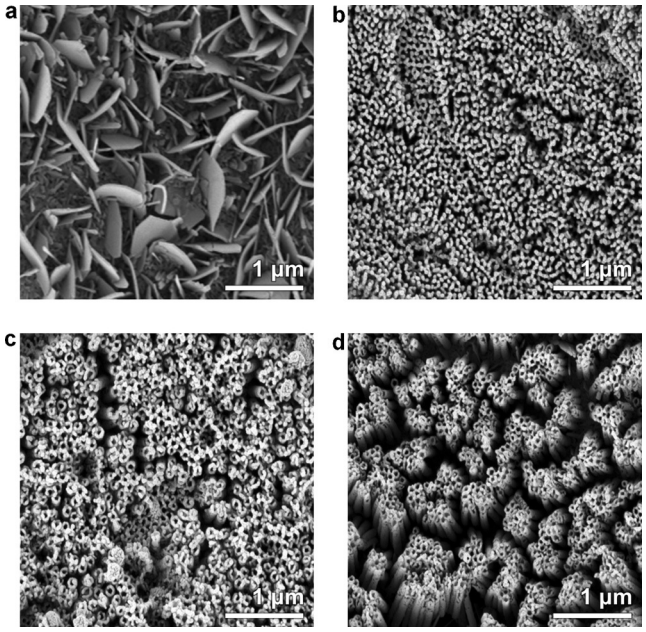

Figure 2. SEM images of iron oxide nanostructures prepared by anodization of iron foil at 50 V for 1 h using ethylene glycol electrolytes of various compositions described in Table S1: a) 0.125 wt% NH_4F and 1.0 vol% H_2O, b) 0.250 wt% NH_4F and 2.0 vol% H_2O, c) 0.500 wt% NH_4F and 3.0 vol% H_2O, and d) 1.000 wt% NH_4F and 4.0 vol% H_2O.

potential (J–V) curve as shown in Figure 3b. The most notable characteristic of the AFF photoanode was the large photocurrent density. The onset of electrochemical water oxidation of hematite in dark condition is known to be around 1.55 V vs. reversible hydrogen electrode (RHE)[27] and we observed a photocurrent density exceeding 5 mA cm^{-2} before reaching the dark current onset (5.49 ± 0.34 mA cm^{-2} at 1.55 V); this is the highest value yet reported for PEC water splitting employing an iron oxide photoelectrode. This superb performance obtained from the AFF photoanode in water photoelectrolysis can be attributed to the large surface area for light harvesting, two-dimensionally confined semiconductor structure for enhanced charge transport, and three-dimensionally extended current collector with a very low sheet resistance, which was measured to be only 2.4 mΩ square^{-1}. The photocurrent density at 1.23 V vs. RHE calculated from the incident photon-to-current efficiency (IPCE) was 2.30 mA cm^{-2}, which corresponds to that obtained from the J–V curve (2.29 mA cm^{-2}). The photocurrent onset was around 0.79 V vs. RHE as calculated from the averaged result displayed in Figure S5; this is consistent with a previous report wherein anodized Fe foil was used as the photoanode.[28]

In the previous studies of PEC water splitting based on hematite photoelectrodes, a steep increase in current was observed after the photocurrent onset. Subsequently, the current reaches a limiting value that is governed by the light harvesting and charge collection properties of the photoelectrode.[32,33] In contrast, in water photoelectrolysis using an AFF, the J–V curve shows a relatively gentle photocurrent slope after the onset potential (similar to low fill factoring behavior in photovoltaic), and this can be understood as the consequence of severe charge recombinations occuring in the inner part of the nanostructured oxides. The diffusion length of holes in hematite is well known to be around 2–4 nm,[29,32] and thus nanostructure thinner than ≈8 nm are requred for near-complete utilization of photo-generated charge carriers. The thicknesses of nanoflakes and porous nano-oxides beneath the two-dimensional structures exceeded 8 nm and the holes generated in the innermost region of the nanostructured iron oxide were not able to participate in water photooxidation because of recombination with electrons. Our results are in line with previous work by Mohaptra et al. wherein iron oxide nanotubes with wall thicknesses of around 5–20 nm manifested J-V curves with low fill factoring behav-

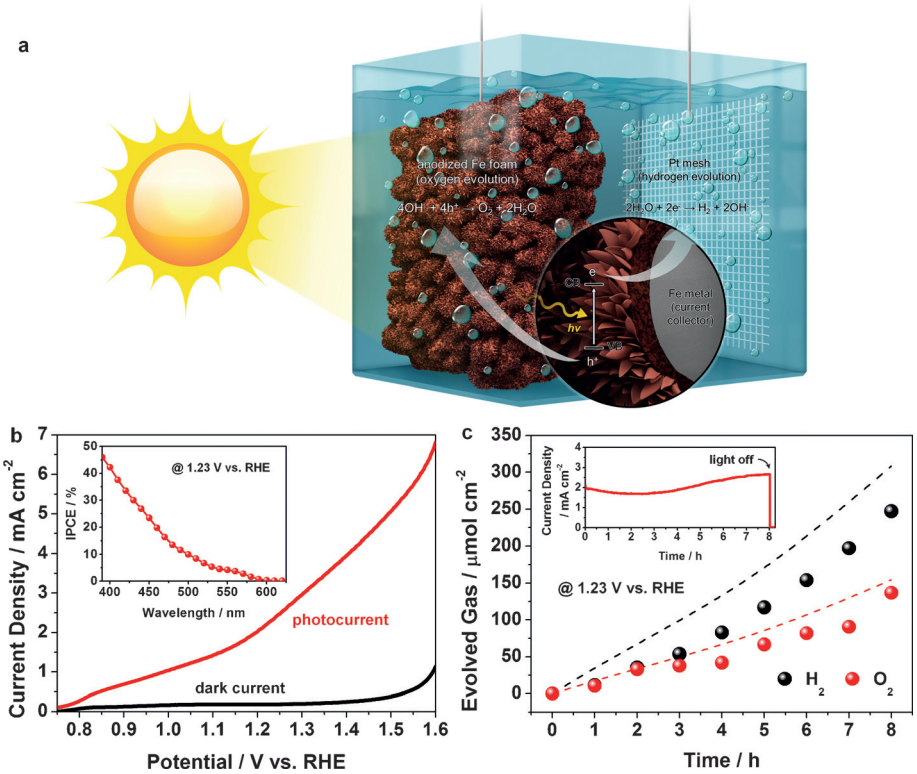

Figure 3. a) Schematic image of the PEC water splitting reaction based on the AFF photoanode. b) J–V characteristic of the AFF photoanode. Inset shows the IPCE data. c) Quantification of gas evolution under AM 1.5G illumination at 1.23 V vs. RHE. The inset shows the photocurrent density during the water splitting reaction and the dashed lines display the amount of gases at 100% Faradaic efficiency.

ior and no indication of limiting photocurrent prior to the dark current onset.[28] Additionally, as can be seen from the transmittance spectrum in Figure S6, the 500 μm thick AFF was completely opaque, suggesting that the rear part of AFF cannot participate in harvesting of photons for water splitting. Therefore, a significant amount of charge recombination at electrode/electrolyte interface takes place in the rear-most region, resulting in the drop of overall performance. However, this also implies that there are possibilities for achiving enhanced performance by optimizing the photoelectrode thickness.

The Faradaic efficiency of the AFF was obtained under AM 1.5G illumination by gas chromatography (GC) analysis. Figure 3c shows the amount of evolved H_2 and O_2 gases at 1.23 V vs. RHE and the corresponding current densities are displayed in the inset. The Faradaic efficiency during 8 h of operation was over 80% (80.1% by H_2 and 88.6% by O_2). Interestingly, photocurrent density increased as the reaction time exceeds 3 h and the evolution rate of H_2 and O_2 gases also increased. The photocurrent surpassed the initial value after 6 h, with Faradaic efficiency being close to unity (97.3%). In order to address this phenomenon, investigations on chemical transition of the photoelectrode were performed. According to the XRD patterns and corresponding Rietveld refinement results of the AFFs before and after the reaction (Figure 4a and Table S2), inactive magnetite was transformed into the active hematite phase with the atomic ratio of hematite/magnetite changed from 1.97 to 2.19. This can be ascribed to an Fe^{3+}/Fe^{2+} transition caused by holes generated from photon absorption.[46] Moreover, changes in chemical states of the AFFs' surface were also characterized by XPS analyses. In the Fe 2p XPS spectra displayed in Figure S7, the $2p_{3/2}$ peak of the bare AFF is located at 710.8 eV and the distance between the $2p_{3/2}$ and $2p_{1/2}$ peaks is 13.6 eV, indicating that the surface of AFF is mainly hematite.[47,48] However, the 2p peaks slightly shift to a lower binding energy after the reaction, attributed to the formation of iron oxyhydroxide (FeOOH) on the surface[47–50] in the basic media. FeOOH is a well-known oxygen evolution catalyst (OEC),[46,50–52] and the FeOOH layer seems to have contributed to the increment of the photocurrent density. Despite these chemical transitions, the morphology of AFFs was maintained after 8 h of water splitting (Figure 4b–e), and this can be attributed to the extremely small thickness (below 1 nm) of the FeOOH layer observable from the TEM images in Figure S8.

For further enhancement in performance, we decorated the surface of AFF with Co OECs by electrodeposition,[53] as schematically illustrated in Figure 5a. Uniform deposition of Co OECs was confirmed by SEM (Figure 5b–e) and TEM analyses (Figure 5f), wherein deposited nanoparticles with lattice spacing of Co (101) are clearly visible, and also by obtaining elemental EDS maps (Figure 5g–i) of the region shown in Figure 5f. Figure 5j displays the performance of PEC water splitting based on the Co-decorated AFF photoanode. Compared to the case of bare AFF, the photocurrent onset was reduced by 0.19 V (an onset of 0.61 was obtained from the averaged results displayed in Figure S9), and the photocurrent density at 1.23 V vs. RHE exceeded 3 mA cm^{-2} with an IPCE value at 400 nm of over 50%. The integrated

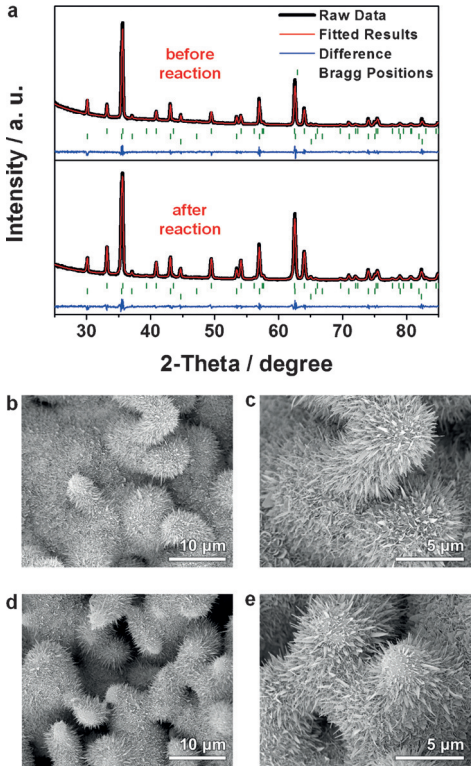

Figure 4. a) XRD patterns and Rietveld refinement results of the AFF photoanodes before and after 8 h of PEC water splitting reaction. b–e) SEM images of AFF photoanode b,c) before and d,e) after 8 h of the PEC water splitting.

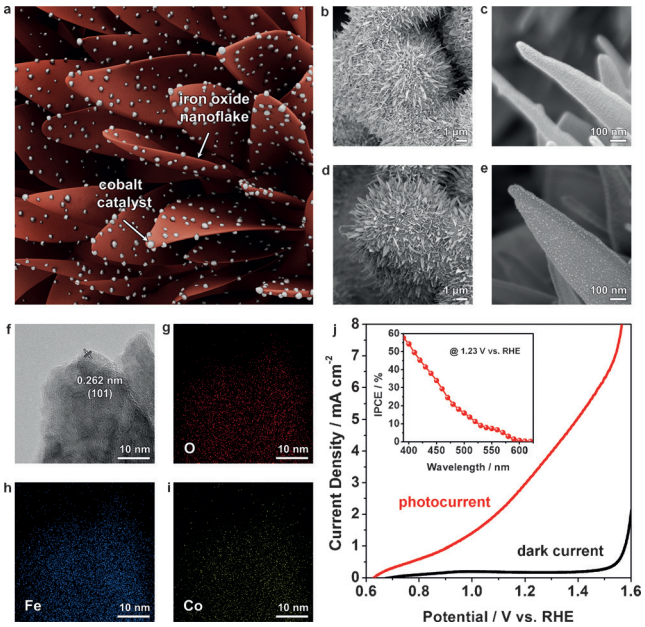

Figure 5. a) Schematic image of the AFF photoanode with Co OECs decorated on the surface. b–e) SEM images of AFFs b,c) before and d,e) after the deposition of Co catalysts. f) TEM image and g–i) elemental EDS g) O, h) Fe, and i) Co maps of Co-decorated AFF. j) *J*–*V* characteristic of the AFF photoanode with Co OECs. The inset shows the IPCE data.

photocurrent density based on the IPCE spectra was 3.06 mA cm^{-2}, a reasonable value considering the 3.25 mA cm^{-2} obtained from the *J–V* result. Also, the photocurrent density reached 6.8 mA cm^{-2} before the dark current onset (6.82 ± 0.53 mA cm^{-2} at 1.55 V); this is the highest value ever reported, to the best of our knowledge, in the case of iron oxide.

In summary, we have constructed an anodized Fe foam photoelectrode for PEC water splitting and verified its superiority by obtaining photocurrent density exceeding 5 mA cm^{-2} (6.8 mA cm^{-2} with Co catalysts) prior to the onset of water electrolysis. The anodized Fe foam is promising because it has ideal characteristics such as a large surface area, low-dimensionally confined semiconductor nanostructure, and three-dimensional metal foam current collector with a very low electrical resistance. Moreover, there is room for further optimization in terms of additional structural/compositional modification and device architecture. These combinations of advantages present in AFF-based PEC water splitting and viabilty for further extension of this design concept to other materials are anticipated to bring advances to the current technology of PEC H_2 production and to the general strategies for utilization of solar energy in various electrocatalyses that are thermodynamically uphill.

Acknowledgements

Y.-E.S. acknowledges financial support from the Institute for Basic Science (IBS) in the Republic of Korea (Project Code: IBS-R006-G1). H.C. acknowledges supports from the Basic Science Research Program (2014R1A2A1A11052513) and Priority (2012-0006680) Research Centers Program through the National Research Foundation (NRF) of the Republic of Korea.

Conflict of interest

The authors declare no conflict of interest.

Keywords: anodization · iron oxide · metal foam · photoelectrochemistry · water splitting

How to cite: *Angew. Chem. Int. Ed.* **2017**, *56*, 6583–6588
Angew. Chem. **2017**, *129*, 6683–6688

[1] J. A. Turner, *Science* **2004**, *305*, 972–974.
[2] N. S. Lewis, D. G. Nocera, *Proc. Natl. Acad. Sci. USA* **2006**, *103*, 15729–15735.
[3] H. B. Gray, *Nat. Chem.* **2009**, *1*, 7.
[4] M. G. Walter, E. L. Warren, J. R. McKone, S. W. Boettcher, Q. Mi, E. A. Santori, N. S. Lewis, *Chem. Rev.* **2010**, *110*, 6446–6473.
[5] X. Chen, L. Liu, P. Y. Yu, S. S. Mao, *Science* **2011**, *331*, 746–750.
[6] J. Luo, J.-H. Im, M. T. Mayer, M. Schreier, M. K. Nazeeruddin, N.-G. Park, S. D. Tilley, H. J. Fan, M. Grätzel, *Science* **2014**, *345*, 1593–1596.
[7] M. Reza Gholipour, C.-T. Dinh, F. Béland, T.-O. Do, *Nanoscale* **2015**, *7*, 8187–8208.
[8] J.-W. Schüttauf, M. A. Modestino, E. Chinello, D. Lambelet, A. Delfino, D. Dominé, A. Faes, M. Despeisse, J. Bailat, D. Psaltis, C. Moser, C. Ballif, *J. Electrochem. Soc.* **2016**, *163*, F1177–F1181.
[9] J. Jia, L. C. Seitz, J. D. Benck, Y. Huo, Y. Chen, J. W. D. Ng, T. Bilir, J. S. Harris, T. F. Jaramillo, *Nat. Commun.* **2016**, *7*, 13237.
[10] J. R. Swierk, T. E. Mallouk, *Chem. Soc. Rev.* **2013**, *42*, 2357–2387.
[11] T. Hisatomi, J. Kubota, K. Domen, *Chem. Soc. Rev.* **2014**, *43*, 7520–7535.
[12] K. Sivula, R. van de Krol, *Nat. Rev. Mater.* **2016**, *1*, 15010.
[13] A. Fujishima, K. Honda, *Nature* **1972**, *238*, 37–38.
[14] W. J. Youngblood, S.-H. A. Lee, Y. Kobayashi, E. A. Hernandez-Pagan, P. G. Hoertz, T. A. Moore, A. L. Moore, D. Gust, T. E. Mallouk, *J. Am. Chem. Soc.* **2009**, *131*, 926–927.
[15] G. Wang, H. Wang, Y. Ling, Y. Tang, X. Yang, R. C. Fitzmorris, C. Wang, J. Z. Zhang, Y. Li, *Nano Lett.* **2011**, *11*, 3026–3033.
[16] H.-i. Kim, D. Monllor-Satoca, W. Kim, W. Choi, *Energy Environ. Sci.* **2015**, *8*, 247–257.
[17] C. Santato, M. Odziemkowski, M. Ulmann, J. Augustynski, *J. Am. Chem. Soc.* **2001**, *123*, 10639–10649.
[18] W. Li, P. Da, Y. Zhang, Y. Wang, X. Lin, X. Gong, G. Zheng, *ACS Nano* **2014**, *8*, 11770–11777.
[19] J. Azevedo, L. Steier, P. Dias, M. Stefik, C. T. Sousa, J. P. Araújo, A. Mendes, M. Graetzel, S. D. Tilley, *Energy Environ. Sci.* **2014**, *7*, 4044–4052.
[20] A. A. Dubale, C.-J. Pan, A. G. Tamirat, H.-M. Chen, W.-N. Su, C.-H. Chen, J. Rick, D. W. Ayele, B. A. Aragaw, J.-F. Lee, Y.-W. Yang, B.-J. Hwang, *J. Mater. Chem. A* **2015**, *3*, 12482–12499.
[21] H. S. Park, K. E. Kweon, H. Ye, E. Paek, G. S. Hwang, A. J. Bard, *J. Phys. Chem. C* **2011**, *115*, 17870–17879.
[22] W. J. Jo, J.-W. Jang, K.-J. Kong, H. J. Kang, J. Y. Kim, H. Jun, K. P. S. Parmar, J. S. Lee, *Angew. Chem. Int. Ed.* **2012**, *51*, 3147–3151; *Angew. Chem.* **2012**, *124*, 3201–3205.
[23] M. Zhou, H. B. Wu, J. Bao, L. Liang, X. W. Lou, Y. Xie, *Angew. Chem. Int. Ed.* **2013**, *52*, 8579–8583; *Angew. Chem.* **2013**, *125*, 8741–8745.
[24] A. Kay, I. Cesar, M. Grätzel, *J. Am. Chem. Soc.* **2006**, *128*, 15714–15721.
[25] S. D. Tilley, M. Cornuz, K. Sivula, M. Grätzel, *Angew. Chem. Int. Ed.* **2010**, *49*, 6405–6408; *Angew. Chem.* **2010**, *122*, 6549–6552.
[26] S. C. Warren, K. Voïtchovsky, H. Dotan, C. M. Leroy, M. Cornuz, F. Stellacci, C. Hébert, A. Rothschild, M. Grätzel, *Nat. Mater.* **2013**, *12*, 842–849.
[27] K. Sivula, R. Zboril, F. Le Formal, R. Robert, A. Weidenkaff, J. Tucek, J. Frydrych, M. Grätzel, *J. Am. Chem. Soc.* **2010**, *132*, 7436–7444.
[28] S. K. Mohapatra, S. E. John, S. Banerjee, M. Misra, *Chem. Mater.* **2009**, *21*, 3048–3055.
[29] K. Sivula, F. Le Formal, M. Grätzel, *ChemSusChem* **2011**, *4*, 432–449.
[30] J. Y. Kim, G. Magesh, D. H. Youn, J.-W. Jang, J. Kubota, K. Domen, J. S. Lee, *Sci. Rep.* **2013**, *3*, 2681.
[31] F. Le Formal, S. R. Pendlebury, M. Cornuz, S. D. Tilley, M. Grätzel, J. R. Durrant, *J. Am. Chem. Soc.* **2014**, *136*, 2564–2574.
[32] A. G. Tamirat, J. Rick, A. A. Dubale, W.-N. Su, B.-J. Hwang, *Nanoscale Horiz.* **2016**, *1*, 243–267.
[33] S. Shen, S. A. Lindley, X. Chen, J. Z. Zhang, *Energy Environ. Sci.* **2016**, *9*, 2744–2775.
[34] A. B. Murphy, P. R. F. Barnes, L. K. Randeniya, I. C. Plumb, I. E. Grey, M. d. Horne, J. A. Glasscock, *Int. J. Hydrogen Energy* **2006**, *31*, 1999–2017.
[35] S. Deville, *Adv. Eng. Mater.* **2008**, *10*, 155–169.
[36] A. A. Plunk, D. C. Dunand, *Mater. Lett.* **2017**, *191*, 112–115.
[37] M. Paulose, K. Shankar, S. Yoriya, H. E. Prakasam, O. K. Varghese, G. K. Mor, T. A. Latempa, A. Fitzgerald, C. A. Grimes, *J. Phys. Chem. B* **2006**, *110*, 16179–16184.

[38] S. Yoriya, H. E. Prakasam, O. K. Varghese, K. Shankar, M. Paulose, G. K. Mor, T. J. Latempa, C. A. Grimes, *Sens. Lett.* **2006**, *4*, 334 – 339.
[39] H. E. Prakasam, O. K. Varhese, M. Paulose, G. P. Mor, C. A. Grimes, *Nanotechnology* **2006**, *17*, 4285 – 4291.
[40] T. J. LaTempa, X. Feng, M. Paulose, C. A. Grimes, *J. Phys. Chem. C* **2009**, *113*, 16293 – 16298.
[41] P. Roy, S. Berger, P. Schmuki, *Angew. Chem. Int. Ed.* **2011**, *50*, 2904 – 2939; *Angew. Chem.* **2011**, *123*, 2956 – 2995.
[42] K. S. Raja, T. Gandhi, M. Misra, *Electrochem. Commun.* **2007**, *9*, 1069 – 1076.
[43] J. H. Lim, J. Choi, *Small* **2007**, *3*, 1504 – 1507.
[44] J. Wu, L. Liu, S. Liu, P. Yu, Z. Zheng, M. Shafa, Z. Zhou, H. Li, H. Ji, Z. M. Wang, *Nano Lett.* **2014**, *14*, 6002 – 6009.
[45] D. M. Knotter, *J. Am. Chem. Soc.* **2000**, *122*, 4345 – 4351.
[46] J. A. Seabold, K.-S. Choi, *J. Am. Chem. Soc.* **2012**, *134*, 2186 – 2192.
[47] G. C. Allen, M. T. Curtis, A. J. Hooper, P. M. Tucker, *J. Chem. Soc. Dalton Trans.* **1974**, 1525 – 1530.
[48] N. S. McIntyre, D. G. Zetaruk, *Anal. Chem.* **1977**, *49*, 1521 – 1529.
[49] A. P. Grosvenor, B. A. Kobe, M. C. Biesinger, N. S. McIntyre, *Surf. Interface Anal.* **2004**, *36*, 1564 – 1574.
[50] J. Y. Kim, D. H. Youn, K. Kang, J. S. Lee, *Angew. Chem. Int. Ed.* **2016**, *55*, 10854 – 10858; *Angew. Chem.* **2016**, *128*, 11012 – 11016.
[51] T. W. Kim, K.-S. Choi, *Science* **2014**, *343*, 990 – 994.
[52] W. D. Chemelewski, H.-C. Lee, J.-F. Lin, A. J. Bard, C. B. Mullins, *J. Am. Chem. Soc.* **2014**, *136*, 2843 – 2850.
[53] Q. Liu, J. He, T. Yao, Z. Sun, W. Cheng, S. He, Y. Xie, Y. Peng, H. Cheng, Y. Sun, Y. Jiang, F. Hu, Z. Xie, W. Yan, Z. Pan, Z. Wu, S. Wei, *Nat. Commun.* **2014**, *5*, 5122.

Manuscript received: March 30, 2017
Version of record online: May 4, 2017

